Christian Löw*, Esben M. Quistgaard, Michael Kovermann, Madhanagopal Anandapadamanaban, Jochen Balbach and Pär Nordlund*

Structural basis for PTPA interaction with the invariant C-terminal tail of PP2A

Abstract: Protein phosphatase 2A (PP2A) is a highly abundant heterotrimeric Ser/Thr phosphatase involved in the regulation of a variety of signaling pathways. The PP2A phosphatase activator (PTPA) is an ATP-dependent activation chaperone, which plays a key role in the biogenesis of active PP2A. The C-terminal tail of the catalytic subunit of PP2A is highly conserved and can undergo a number of posttranslational modifications that serve to regulate the function of PP2A. Here we have studied structurally the interaction of PTPA with the conserved C-terminal tail of the catalytic subunit carrying different posttranslational modifications. We have identified an additional interaction site for the invariant C-terminal tail of the catalytic subunit on PTPA, which can be modulated *via* posttranslational modifications. We show that phosphorylation of $Tyr307_{PP2A-C}$ or carboxymethylation of $Leu309_{PP2A-C}$ abrogates or diminishes binding of the C-terminal tail, whereas phosphorylation of $Thr304_{PP2A-C}$ is of no consequence. We suggest that the invariant C-terminal residues of the catalytic subunit can act as affinity enhancer for different PP2A interaction partners, including PTPA, and a different 'code' of posttranslational modifications can favour interactions to one subunit over others.

Introduction

Protein phosphatase 2A (PP2A) is a heterotrimeric Ser/Thr phosphatase with multiple functions in various signaling pathways (Mumby and Walter, 1993; Hunter, 1995; Gallego and Virshup, 2005; Sablina et al., 2010; Wurzenberger and Gerlich, 2011; Heijman et al., 2013). It is highly abundant and conserved throughout eukaryotic species. A modular architecture in combination with complex regulation forms the basis of its broad functional diversity. PP2A holoenzymes consist of a core dimer, which contains the structural A subunit (also known as scaffolding subunit; two isoforms α and β) and a catalytic C subunit (two isoforms α and β), which assemble with various classes of regulatory B-subunits to form the heterotrimeric complex (Janssens et al., 2008; Shi, 2009a,b; Lambrecht et al., 2013; Sents et al., 2013). Four families of regulatory B-subunits, with no homology between them, have been identified to date: B/B55/PR55, B'/B56/PR61, B"/PR72, and B'''/Striatin/PR93 (Shi, 2009a,b; Virshup and Shenolikar, 2009). Within the holoenzyme, the regulatory B-subunits control the function of PP2A by mediating substrate specificity and modulating the catalytic activity. Crystal structures of the regulatory B, B', and B" subunits in isolation or in complex with the PP2A core dimer and other PP2A interacting and activating proteins have been determined and gave ideas how regulatory subunits might recognize different substrates and affect and influence PP2A activity (Groves et al., 1999; Chao et al., 2006; Leulliot et al., 2006; Xing et al., 2006, 2008; Xu et al., 2006, 2008; Chen et al., 2007; Cho and Xu, 2007; Cho et al., 2007; Huhn et al., 2009; Magnusdottir et al., 2009; Stanevich et al., 2011; Tsai et al., 2011; Jiang et al., 2013; Wlodarchak et al., 2013; Guo et al., 2014).

*Corresponding authors: Christian Löw, Karolinska Institutet, Department of Medical Biochemistry and Biophysics, Scheeles väg 2, S-17177 Stockholm, Sweden; and European Molecular Biology Laboratory, Hamburg Outstation c/o DESY, Notkestrasse 85, 22603 Hamburg, Germany; and **Pär Nordlund,** Karolinska Institutet, Department of Medical Biochemistry and Biophysics, Scheeles väg 2, S-17177 Stockholm, Sweden; and School of Biological Sciences, Nanyang Technological University, 639798 Singapore, Singapore, e-mail: christian.low@ki.se, par.nordlund@ki.se
Esben M. Quistgaard: Karolinska Institutet, Department of Medical Biochemistry and Biophysics, Scheeles väg 2, S-17177 Stockholm, Sweden
Michael Kovermann and Jochen Balbach: Fachgruppe Biophysik, Institut für Physik, Martin-Luther-Universität Halle-Wittenberg, Betty-Heimann-Strasse 7, D-06120 Halle/Saale, Germany
Madhanagopal Anandapadamanaban: Karolinska Institutet, Department of Medical Biochemistry and Biophysics, Scheeles väg 2, S-17177 Stockholm, Sweden; and Department of Physics, Chemistry and Biology, Linköping University, S-58183 Linköping, Sweden

The biogenesis of active PP2A including the assembly of the subunits is tightly regulated and relies on an activation process of the catalytic C-subunit involving additional modulators and/or posttranslational modifications (Sents et al., 2013). Here the PP2A phosphatase activator (PTPA) plays an essential role as an ATP-dependent activation chaperone (Guo et al., 2014). PTPA was originally identified as an ATP/Mg^{2+}-dependent upregulator of phosphotyrosyl phosphatase activity of PP2A *in vitro* (Cayla et al., 1994) but has later been shown to also be required for full phosphoseryl/threonyl phosphatase activity of newly synthesized catalytic subunits (Fellner et al., 2003). The importance of PTPA is further underlined by its high evolutionary conservation and the fact that deletions of the two PTPA homologues in yeast, Rrd1 and Rrd2, are lethal in certain nutritional backgrounds (Rempola et al., 2000).

The C-terminal tail (residues 304–309: TPDYFL) of the catalytic subunit of PP2A is highly conserved and can undergo a number of posttranslational modifications that serve to regulate the function of PP2A (see Figure 1A) (Janssens and Goris, 2001). Phosphorylation sites at Thr304$_{PP2A-C}$ and Tyr307$_{PP2A-C}$ have mainly been associated with inactivation of PP2A (Chen et al., 1992; Schmitz et al., 2010), whereas methylation of the free C-terminus of Leu309 has been shown to be an absolute prerequisite for the recruitment of certain subunits *in vivo* (e.g., PR55),

but not being strictly required for others (Janssens et al., 2008). This modification is fully reversible; its addition is catalyzed by the enzyme LCMT1, and its removal, by the methylesterase PME-1 (De Baere et al., 1999; Ogris et al., 1999). There is an apparent discrepancy of the importance of this modification between *in vivo* and *in vitro* studies because holoenzymes assemble into stable complexes *in vitro* even in the absence of the C-terminal tail (Xu et al., 2006, 2008; Ikehara et al., 2007; Stanevich et al., 2011). The structural information on PP2A subunits and its complexes is constantly increasing, but the structural role of the C-terminal residues of the catalytic PP2A subunit with their different posttranslational modifications has rarely been addressed. Despite its biochemical importance, the C-terminal residues were either removed for crystallization purposes or not resolved in the crystal structures (except for Cho and Xu, 2007). Although several groups have reported the structure of PTPA a few years ago (Chao et al., 2006; Leulliot et al., 2006; Magnusdottir et al., 2009), including us, its detailed functional role and corresponding PP2A binding interfaces remained elusive until recently, when a structure of PTPA in complex with the PP2A core dimer unraveled the structural and functional role of PTPA as ATP-dependent activation chaperone. However, also here, the construct of the catalytic subunit used for crystallization was lacking the C-terminal residues. In the present
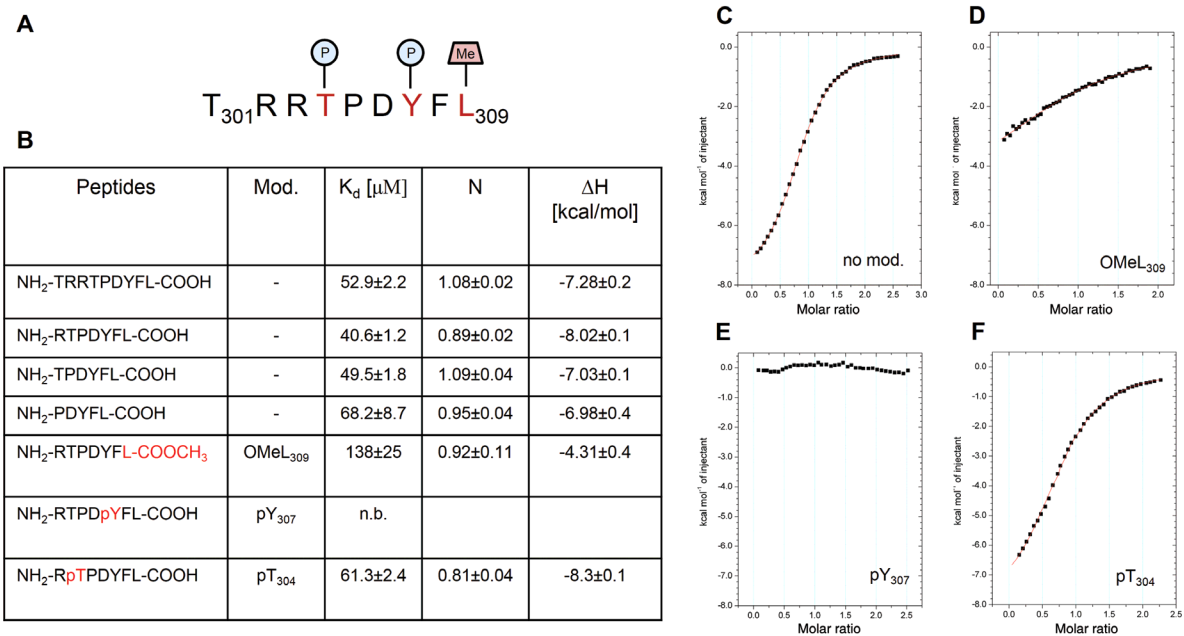

Figure 1 Interaction of PTPA with the C-terminal peptide of the catalytic subunit of PP2A.
(A) Sequence and known modifications of the invariant C-terminus of the catalytic subunit. (B) Resulting binding properties of peptides of various lengths and with different modifications to PTPA are shown. (C–F) Integrated heat changes upon binding of peptides with different modifications (shown in the different panels) to PTPA are plotted against the peptide/PTPA concentration ratio. n.b., no binding detected.

Peptides	Mod.	K_d [μM]	N	ΔH [kcal/mol]
NH$_2$-TRRTPDYFL-COOH	-	52.9±2.2	1.08±0.02	-7.28±0.2
NH$_2$-RTPDYFL-COOH	-	40.6±1.2	0.89±0.02	-8.02±0.1
NH$_2$-TPDYFL-COOH	-	49.5±1.8	1.09±0.04	-7.03±0.1
NH$_2$-PDYFL-COOH	-	68.2±8.7	0.95±0.04	-6.98±0.4
NH$_2$-RTPDYFL-COOCH$_3$	OMeL$_{309}$	138±25	0.92±0.11	-4.31±0.4
NH$_2$-RTPDpYFL-COOH	pY$_{307}$	n.b.		
NH$_2$-RpTPDYFL-COOH	pT$_{304}$	61.3±2.4	0.81±0.04	-8.3±0.1

work, we have characterized the interaction of the PP2A activation chaperone PTPA with the C-terminal tail of the PP2A catalytic subunit carrying various posttranslational modifications. Only a peptide that is free of posttranslational modifications was able to bind to PTPA in the micromolar range as judged by nulear magnetic resonance (NMR) and isothermal titration calorimetry (ITC) experiments. Binding of the unmodified peptide was further verified by a co-crystal structure of the PTPA/peptide complex, which, for the first time, has identified the interaction site for the C-terminal tail of the catalytic subunit on PTPA and furthermore explains why posttranslational modifications disfavor this interaction. The data presented here thus extend our knowledge about how PTPA interacts with the PP2A catalytic subunit and how this interaction may be modulated by posttranslational modifications.

Results and discussion

PTPA interaction with the C-terminal tail of the catalytic subunit and ATP

To investigate the potential of PTPA for interacting with the C-terminal tail of the catalytic subunit, we used peptides of different length (5–9 amino acids) representing the unmodified C-terminal residues of the catalytic C subunit and studied their interaction with PTPA using ITC (Figure 1B–F). A peptide representing the last 5 amino acids of the invariant C-terminal tail was sufficient to retain micromolar binding affinity, indicating that only these residues are involved in binding. We could not confirm binding of the tetra peptide AAPK, which has recently been co-crystallized with PTPA (Leulliot et al., 2006) but contained additional N- and C-terminal modifications (suc-AAPK-pNa).

Next we used a set of peptides of the same length (7 amino acid residues) of the C-terminal peptide carrying the various posttranslational modifications described for the catalytic subunit; phosphorylation of Thr304$_{PP2A-C}$, phosphorylation of Tyr307$_{PP2A-C}$, and carboxymethylation of Leu309$_{PP2A-C}$ (see Figure 1A). Although the binding isotherm for the peptide carrying a phosphorylation at Thr304$_{PP2A-C}$ was almost identical to the unmodified peptide, phosphorylation of Tyr307$_{PP2A-C}$ abolished binding completely. Carboxymethylation of the C-terminal Leu309$_{PP2A-C}$ residue also reduced binding affinity to PTPA, reflected in a more than 3-fold increase of the K_d value and reduced binding enthalpy. To confirm these data and monitor whether peptide binding induces major conformational changes, we recorded two-dimensional (2D) ^{1}H/^{15}N HSQC spectra of

^{15}N-labeled PTPA in the absence and presence of excess peptide with different modifications (Supplementary Figure 1). Despite its size of more than 35 kDa, the recorded 2D ^{1}H/^{15}N HSQC spectrum of PTPA was of high quality and allowed the identification of more than 270 isolated resonances (out of 288 expected) with minimal signal overlap. Addition of unmodified peptide induced small chemical shift changes of <25 resonances, indicating that no major conformational changes occur upon peptide binding in solution (Supplementary Figure 1).

We further used 2D NMR spectroscopy to characterize binding of ATP to isolated PTPA. Despite some efforts, ATP binding to PTPA in solution could not be shown so far using various biophysical techniques, probably due to the low binding affinity (Magnusdottir et al., 2009). However, NMR titration of PTPA with different amounts of ATP induced chemical shift changes of another set of resonances compared with peptide binding. A number of cross-peaks were followed over the entire titration range and globally analyzed using a 1:1 binding model. The resulting affinity was in the low millimolar range (K_d=4.8±0.3 mM) (see Figure 2). The low binding affinity of isolated PTPA to ATP can now be explained in the context of the recently published crystal structure of PTPA in complex with the PP2A core dimer, which showed that ATP binds in a bipartite binding site contributed by both PTPA and the catalytic subunit. Nevertheless, our data show specific low affinity ATP binding to PTPA in solution, and we conclude that the binding sites for ATP recognition and binding of the C-terminal peptide of the catalytic subunit are different because they induce chemical shift changes of a different set of backbone amide resonances.

Crystal structure of PTPA in complex with the C-terminal tail of the catalytic subunit

To obtain high-resolution insights into how the C-terminal residues of the catalytic subunit interact with PTPA, we crystallized PTPA with a peptide (unmodified) that corresponds to the last 6 amino acids of the catalytic subunit. Crystals were obtained under similar conditions as the apo structure described previously (Magnusdottir et al., 2009). Two molecules of PTPA were found in the asymmetric unit using molecular replacement, and the structure was refined at 1.8 Å (Table 1). The structure is almost identical to the previously determined structures [root mean square deviations (RMSD)=0.227 Å over 1974 atoms for superimposing chain A on PDB:2G62], except for the presence of the co-crystallized peptide, for which 5 of 6 residues could be modeled (Figure 3). The three C-terminal residues of
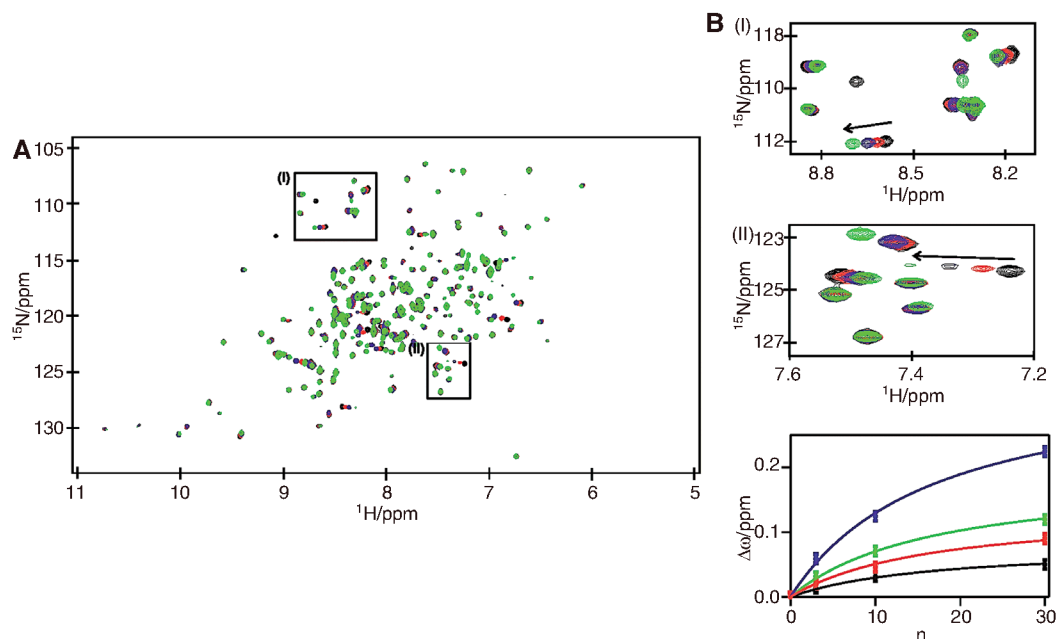
Figure 2 PTPA interaction with ATP.

(A) Overlay of 2D ^{1}H-^{15}N TROSY-HSQC spectra of ^{15}N PTPA acquired at T=298 K and B_{0}=18.8 T in the absence (black) and in presence of different amounts of ATP (red, n=3; blue, n=10; green, n=30). (B) Close-up views of superimposed NMR spectra showing major chemical shift changes upon ATP binding (I, II) and global data regression of four residues showing largest changes of chemical shifts (determined according to Grzesiek et al., 1996) leading to binding affinity of K_{d}=4.8±0.3 mM assuming a one-to-one binding model.

the peptide (i.e., residues Tyr307$_{PP2A-C}$, Phe308$_{PP2A-C}$, and Leu309$_{PP2A-C}$) bind to PTPA in a small hydrophobic groove formed between the two C-terminal α-helices α12 (residues 273–278) and α13 (residues 284–298) (Figure 3A). Notably, the same site was also found to bind part of the uncleaved tobacco etch virus (TEV)-linker region from a symmetry-related mate in one of the formerly determined PTPA structures (Magnusdottir et al., 2009). In this groove, the side chains of Tyr307$_{PP2A-C}$ and Phe308$_{PP2A-C}$ establish hydrophobic interactions and van der Waals interactions with Ile278, Val287, Gly290, Met294, and Ala297 (Figure 3B). Disruption of this binding groove by introducing a negative charge in position 290 of PTPA (mutant G290D) led to a complete loss of binding of the modification free C-terminal peptide (Supplementary Figure 2). In addition, a number of electrostatic interactions and hydrogen bonds are also formed. The C-terminal carboxylate of Leu309$_{PP2A-C}$ forms electrostatic interactions with a basic ridge formed by helix α13 and encompassing residues Lys286 and Arg293 (Figure 3A and C), and Tyr307$_{PP2A-C}$ is in close hydrogen bonding distance to the guanidinium group of Arg293 (*via* its main chain carboxylate) and the side chain of Glu298 (*via* its side chain hydroxyl group) (Figure 3C).

These observations are in good agreement with the results from binding experiments. The structure thus suggests that phosphorylation of Tyr307$_{PP2A-C}$ would result in

severe steric and electrostatic clashes with Glu298 and that carboxymethylation of Leu309$_{PP2A-C}$ would clash with Arg293, explaining why these modifications abrogate or diminish binding. This is further confirmed by mutational analysis, where binding of the modification free C-terminal peptide is strongly reduced to the PTPA mutant R293A (Supplementary Figure 2). Residues Pro305$_{PP2A-C}$ and Asp306$_{PP2A-C}$ were poorly defined in the electron density (Figure 3C) and probably do not significantly contribute to binding with PTPA. Indeed, these two residues have different conformations in the two molecules in the asymmetric unit, further supporting the notion that they are more flexible and of no major importance for binding (Figure 3D). Therefore, it is not surprising that we found phosphorylation of Thr304$_{PP2A-C}$ to have no measureable impact on binding affinity. Interestingly, Leu309$_{PP2A-C}$ was also modeled slightly differently in the two molecules (Figure 3D). In the B molecule, interaction with Lys286 thus seems weaker than in the A molecule (salt bridge distances of 4.2 and 2.8 Å, respectively), suggesting that this salt bridge may be less important than that formed with Arg293.

The previously proposed binding interface of PTPA with the catalytic subunit of PP2A based on mutational data (Chao et al., 2006) has now been confirmed by the recent PTPA-PP2A complex structure (Guo et al., 2014), except that three residues that were reported to be

Table 1 Data processing and refinement statistics.

	PTPA:PPP2CA C-terminal peptide
Data collection	
Beamline	Diamond I24
Wavelength (Å)	0.9687
Space group	P1
Cell dimensions	
a, b, c (Å)	43.67, 47.97, 87.18
α, β, γ (°)	84.41 80.23 88.23
Resolution (Å)	29.17–1.80 (1.84–1.80)
R_{sym}	0.150 (0.665)
$I/\sigma I$	8.08 (2.30)
Completeness (%)	97.0 (86.6)
Total no. reflections	313 580 (18 655)
Redundancy	5.0 (4.5)
Wilson B-factor (Å²)	16.5
Refinement	
R_{work}/R_{free}	0.158/0.186
No. atoms	5761
Protein	4890
Peptides	94
Solvent (water)	703
Solvent (other)	74
B-factors	
Protein	19.2
Peptides	38.1
Solvent	34.4
RMSD	
Bond lengths (Å)	0.003
Bond angles (°)	0.851
Ramachandran plot	
Favored (%)	97.3
Outliers (%)	0.0

Numbers in parentheses refer to statistics for the outer shell.

relevant for binding (Val281, Gly290, Met294) were found to be rather distant from the PTPA-PP2AC binding site in the complex structure. It should be noted, however, that a catalytic subunit construct lacking the C-terminal tail was used for crystallization of the complex. Our work now offers an explanation for the role of Val281/Gly290/Met294 that is in agreement with all available data, as we find that they are indeed involved in binding or close to the binding site, but engage the C-terminal tail, which was missing in the complex structure (Figure 4). Mutating Gly290 or Met294 into aspartates (Chao et al., 2006) would result in clashes with $Phe308_{PP2A-C}$ and $Tyr307_{PP2A-C}$, respectively, and reduce the overall binding affinity by abrogating binding of the C-terminal tail as shown.

Conclusion

In summary, we have identified the interaction site for the invariant C-terminal tail of the catalytic subunit on PTPA,

and our study thus complements the study by Guo et al. (2014) and deepens our understanding of how PTPA interacts with PP2A (Figure 4). We furthermore find that binding of the C-terminal tail can be modulated *via* posttranslational modifications; phosphorylation of $Tyr307_{PP2A-C}$ or carboxymethylation of $Leu309_{PP2A-C}$ thus both abrogate or diminish binding of the C-terminal tail, whereas phosphorylation of $Thr304_{PP2A-C}$ is of no consequence. Phosphorylation of $Tyr307_{PP2A-C}$ has been described together with inactivation of PP2A. Based on our findings here, we can speculate that this inactivation is caused by preventing its activation by PTPA. The role of PTPA as an activation chaperone in the biogenesis pathway of newly synthesized, unmodified, and inactive PP2A is also supported by the observation that the isolated posttranslational free tail of the catalytic subunit of PP2A is bound with the highest affinity. The importance of this interaction needs to be further confirmed in the context of full length PP2A combined with functional studies in the future.

We suggest that the invariant C-terminal tail of the catalytic subunit provides an additional binding site, which can act as affinity enhancer for different PP2A interaction partners, including PTPA, and a different 'code' of posttranslational modifications can favor interactions to one subunit over others. This makes sense in the context of a cellular environment where multiple potential binding partners are present at a time and fine-tuning *via* posttranslational modifications allows for a fast regulation of various multi-subunit assemblies and thus fine-tuning of the overall activity and specificity of PP2A.

Materials and methods

Materials and reagents

Isopropyl-β-D-thiogalactopyranoside (IPTG) was purchased from Affymetrix (Maumee, OH, USA). Lysogeny broth medium was from Becton Dickinson (Franklin Lakes, NJ, USA) and terrific broth (TB) was from Formedium (Norfolk, UK). All used peptides were purchased from either GenScript (Piscataway, NJ, USA) or GL Biochem (Shanghai, China). The sequences of all used peptides are given in the table of Figure 1. Crystallization reagents were from Qiagen (Germantown, MD, USA). All other chemicals were of analytical grade and obtained from Sigma-Aldrich (St. Louis, MO, USA), unless otherwise stated.

Gene construction protein expression and purification

The sequence of full-length human PTPA (residues 1–323) (UniProt: Q15257-2, isoform 1) and a deletion construct (residues 22–323) were
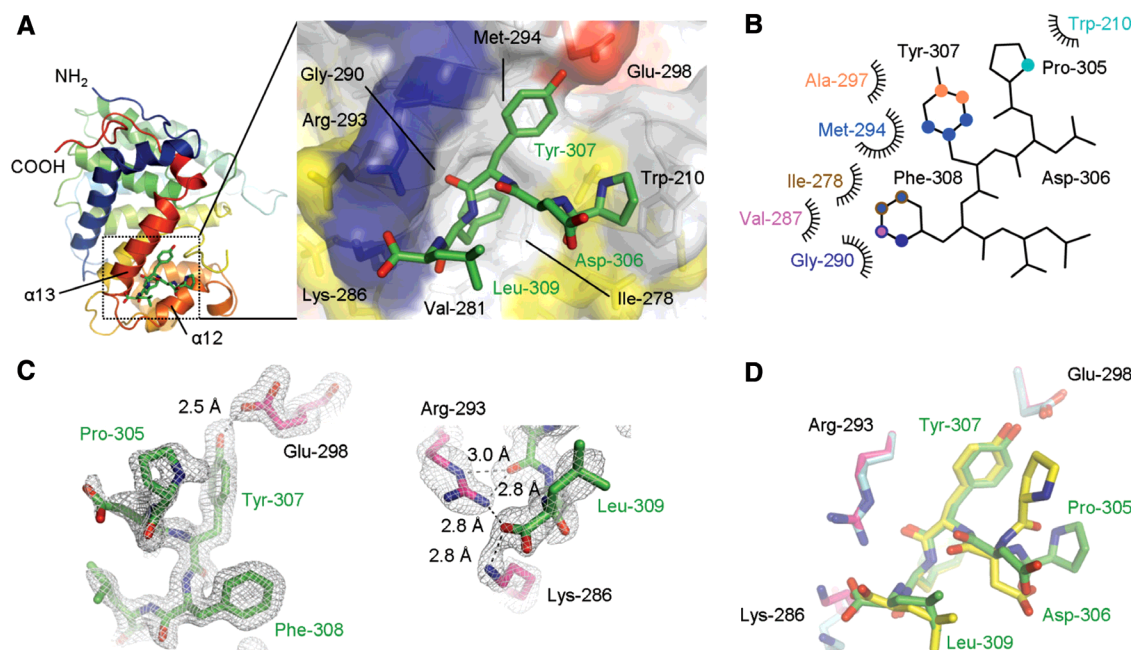
Figure 3 Binding of the C-terminal tail of the PP2A catalytic subunit to PTPA.
(A) Overview of binding site. (Left) Location of the binding site between α12 and α13. PTPA is colored 'rainbow' (N-terminal blue, C-terminal red), and the bound peptide is shown as green sticks. (Right) Zoomed view of binding site. Here, PTPA is colored by amino acid type (acidic, red; basic, blue; polar, yellow; hydrophobic, gray). (B) LigPlot schematic showing van der Waal interactions between the peptide and PTPA. Interacting PTPA residues are annotated and labeled in different colors. Interacting atoms in the peptide are marked with dots having the same color(s) as the PTPA residues with which they interact. (C) Hydrogen bonds and salt bridges. PTPA is purple and the peptide green. Two views are presented. Interactions are shown as stippled lines, and their lengths are indicated. The 1σ 2Fo-Fc map is also shown (gray mesh). (D) Overlay of the binding sites of the two molecules of PTPA in the asymmetric unit. The A molecule is purple with bound peptide (chain C) in green, and the B molecule is light blue with bound peptide (chain D) in yellow. The electron density map was best for the A/C complex, and this complex was therefore used for generating all other images.

cloned into the pET-based pNIC28-Bsa4 expression vector as an N-terminal His$_6$ fusion with a TEV cleavage site between the tag and the protein (Woestenenk et al., 2004; Graslund et al., 2008). Expression of PTPA was induced in *Escherichia coli* BL21ΔSlyD(DE3) grown in TB medium at 37°C with 0.2 mM IPTG (Quistgaard et al., 2012). The temperature was reduced to 20°C, and cells were harvested 18 h after induction. After cell lysis, the supernatant was loaded on a nickel-nitrilotriacetate (Ni-NTA) immobilized metal ion affinity chromatography (IMAC) column and washed with wash buffer containing 20 mM imidazole and 40 mM imidazole [20 mM sodium phosphate, 300 mM NaCl, 0.5 mM Tris(2-carboxyethyl)phosphine (TCEP), 5% glycerol, and 20–40 mM imidazole, pH 7.5] over 25 column volumes and eluted with 20 mM sodium phosphate; 150 mM NaCl; 0.5 mM TCEP, 5% glycerol, and 300 mM imidazole (pH 7.5). The N-terminal histidine-tag was cleaved off overnight after buffer exchange (20 mM sodium phosphate, pH 7.5, 300 mM NaCl, 0.5 mM TCEP, and 5% glycerol) with 0.1 mg TEV protease/mg protein. After a reverse IMAC step, the cleaved protein was then further purified by preparative gel filtration in either 20 mM HEPES (pH 7.5), 100 mM NaCl, 0.5 mM TCEP, and 5% glycerol or 20 mM sodium phosphate, 100 mM NaCl, 0.5 mM TCEP (Löw et al., 2012). The purified protein was >99% pure and devoid of any obvious contaminations. The same methods were used for the purification of the full-length protein and the deletion construct expressed in full and minimal medium. Isotopically labeled ^{15}N NMR samples were produced using M9 minimal media based on ^{15}NH$_4$Cl

as nitrogen source (Cambridge Isotope Laboratories, Inc., Tewksbury, MA, USA) and supplemented with vitamin mix. Mutations in PTPA were introduced following the Quikchange strategy, and mutants were expressed and purified as the wild-type protein.

Crystallization and structure determination

To form the complex for crystallization, human PTPA (construct spanning residues 22–323) was mixed with a 2-fold excess of the hexapeptide NH$_2$-TPDYFL-COOH and incubated for at least 1 h before crystallization trials (total protein concentration of 20 mg/ml). Crystals of the PTPA/peptide complex grew in 2 M (NH$_4$)$_2$SO$_4$, 0.1 M HEPES, pH 7.5, in 96-well sitting-drop plates at 4°C within 4 weeks.

The crystals were flash-frozen in liquid nitrogen after addition of cryosolution (original crystallization solution with additional 20% glycerol) to the crystallization drop. Data were then collected at beamline I24 at Diamond Light Source (Oxford, UK) and processed with XDS and XSCALE (Kabsch, 2010). The crystals belonged to space group P1, so to improve completeness, we scaled two data sets together from different crystals. A molecular replacement solution was found with Phaser (McCoy et al., 2007) using the apo PTPA structure reported previously (2G62.pdb; Magnusdottir et al., 2009). Initial model building and refinement were performed using the
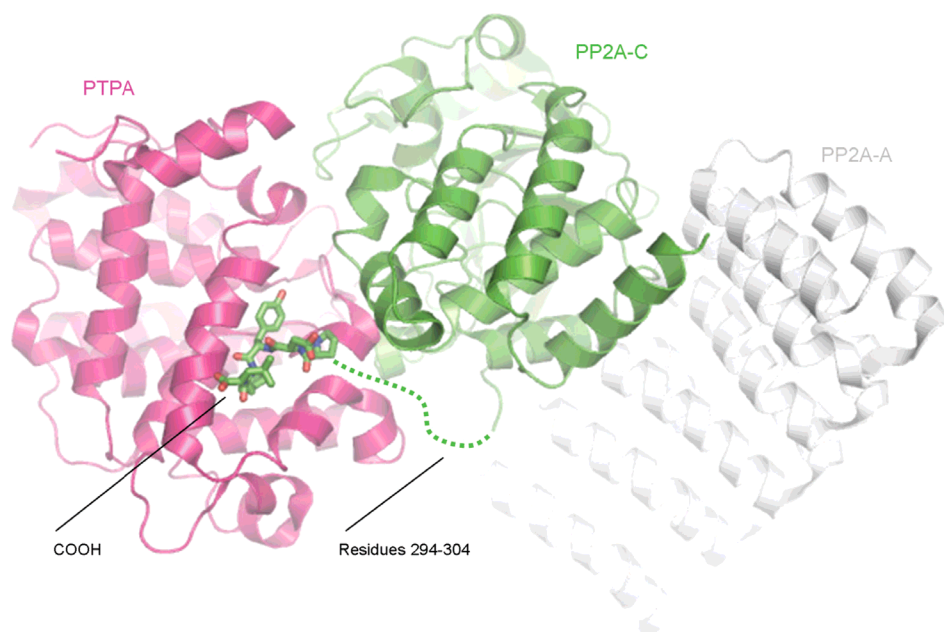
Figure 4 Model of the PP2A-PTPA complex.
Overview of how PTPA interacts with the PP2A core dimer. The structure of PTPA in complex with the C-terminal tail of the catalytic subunit (PDB:4NY3; this work) was superimposed on the structure of the ternary complex consisting of PTPA, scaffolding subunit (PP2A-A) and PP2A catalytic subunit (PP2A-C) lacking the C-terminal tail (PDB:4LAC). PTPA from 4NY3 is shown in pink cartoon, PP2A-A from 4LAC is shown in gray cartoon, PP2A-C without the C-terminal tail from 4LAC is shown in green cartoon, and the PP2A-C C-terminal tail from 4NY3 is shown as green sticks.

AutoRickshaw pipeline. The structure was then refined by multiple cycles of manual rebuilding in Coot (Emsley et al., 2010) and maximum likelihood refinement with phenix refine (Table 1). The model was validated using MolProbity (97.3% favored in Ramachandran plot; overall MolProbity score 1.11; 100th percentile) (Chen et al., 2010). We used PyMol for structure superimpositions and structure figures (DeLano, 2003). Coordinates and structure factors have been deposited in the PDB with the accession number 4NY3.

Peptide binding experiments using ITC

ITC measurements were performed on an iTC200 or VP-ITC instrument (GE Healthcare, Chalfont St. Giles, UK). Purified tag-free full-length PTPA at a concentration of 100–320 μM in the calorimetric cell (total cell volume of ~220/1400 μl) was titrated with various peptides representing the C-terminus of the catalytic subunit of PP2A, varying in length and posttranslational modifications at a concentration of 1–4 mM (15–50 injections) at 20°C. As buffer, 20 mM HEPES (pH 7.5) with 100 mM NaCl, 5% glycerol, and 0.5 mM TCEP was used. The heat generated after each ligand injection was obtained by integration of the calorimetric signal. Resulting binding isotherms were analyzed according to a 1:1 binding model using Origin software (OriginLab, Northampton, MA, USA).

NMR spectroscopy

All ^1H and ^1H-^{15}N TROSY-HSQC NMR spectra were acquired with a Bruker Avance III 600- or 800-MHz spectrometer using a 5 -mm room temperature (600 MHz) or cryoprobe (800 MHz) with z-gradients in 20 mM sodium phosphate buffer (pH 7.5), 100 mM NaCl, 0.5 mM TCEP containing 10% ^2H_2O at 20°C. Protein concentration was 0.3–0.5 mM for all measurements in the presence of excess peptide. PTPA titration experiments were carried out by successive addition of aliquots of a stock solution of ATP/Mg^{2+} in the same buffer as the protein. Complex formation was monitored by recording a 2D ^1H/^{15}N TROSY-HSQC spectrum after each titration step. The mean weighted difference in chemical shifts was calculated according to the following equation: $\Delta\delta_{MW}(^1H,^{15}N)=\sqrt{\{(\Delta\delta(^1H)^2+1/25\Delta\delta(^{15}N)^2)/2\}}$ (Grzesiek et al., 1996). All two-dimensional spectra were recorded using a sensitivity enhanced version of the TROSY-HSQC approach (Weigelt, 1998). Each TROSY-HSQC spectrum was recorded for 3 h, 20 min (40 scans with 1024/256 data matrix). ^1H-^{15}N spectra were processed by NMRPipe (Delaglio et al., 1995) and analyzed by NMRView (Johnson and Blevins, 1994).

References

Cayla, X., Van Hoof, C., Bosch, M., Waelkens, E., Vandekerckhove, J., Peeters, B., Merlevede, W., and Goris, J. (1994). Molecular cloning, expression, and characterization of PTPA, a protein that activates the tyrosyl phosphatase activity of protein phosphatase 2A. J. Biol. Chem. *269*, 15668–15675.

Chao, Y., Xing, Y., Chen, Y., Xu, Y., Lin, Z., Li, Z., Jeffrey, P.D., Stock, J.B., and Shi, Y. (2006). Structure and mechanism of the phosphotyrosyl phosphatase activator. Mol. Cell *23*, 535–546.

Chen, J., Martin, B.L., and Brautigan, D.L. (1992). Regulation of protein serine-threonine phosphatase type-2A by tyrosine phosphorylation. Science *257*, 1261–1264.

Chen, Y., Xu, Y., Bao, Q., Xing, Y., Li, Z., Lin, Z., Stock, J.B., Jeffrey, P.D., and Shi, Y. (2007). Structural and biochemical insights into the regulation of protein phosphatase 2A by small t antigen of SV40. Nat. Struct. Mol. Biol. *14*, 527–534.

Chen, V.B., Arendall, W.B., 3rd, Headd, J.J., Keedy, D.A., Immormino, R.M., Kapral, G.J., Murray, L.W., Richardson, J.S., and Richardson, D.C. (2010). MolProbity: all-atom structure validation for macromolecular crystallography. Acta Crystallogr. D *66*, 12–21.

Cho, U.S. and Xu, W. (2007). Crystal structure of a protein phosphatase 2A heterotrimeric holoenzyme. Nature *445*, 53–57.

Cho, U.S., Morrone, S., Sablina, A.A., Arroyo, J.D., Hahn, W.C., and Xu, W. (2007). Structural basis of PP2A inhibition by small t antigen. PLoS Biol. *5*, e202.

De Baere, I., Derua, R., Janssens, V., Van Hoof, C., Waelkens, E., Merlevede, W., and Goris, J. (1999). Purification of porcine brain protein phosphatase 2A leucine carboxyl methyltransferase and cloning of the human homologue. Biochemistry *38*, 16539–16547.

Delaglio, F., Grzesiek, S., Vuister, G.W., Zhu, G., Pfeifer, J., and Bax, A. (1995). NMRPipe: a multidimensional spectral processing system based on UNIX pipes. J Biomol. NMR *6*, 277–293.

DeLano, W. (2003). The PyMOL Molecular Graphics System. DeLano Scientific LLC. http://www.pymol.org.

Emsley, P., Lohkamp, B., Scott, W.G., and Cowtan, K. (2010). Features and development of Coot. Acta Crystallogr. D *66*, 486–501.

Fellner, T., Lackner, D.H., Hombauer, H., Piribauer, P., Mudrak, I., Zaragoza, K., Juno, C., and Ogris, E. (2003). A novel and essential mechanism determining specificity and activity of protein phosphatase 2A (PP2A) *in vivo*. Genes Dev. *17*, 2138–2150.

Gallego, M. and Virshup, D.M. (2005). Protein serine/threonine phosphatases: life, death, and sleeping. Curr. Opin. Cell Biol. *17*, 197–202.

Graslund, S., Sagemark, J., Berglund, H., Dahlgren, L.G., Flores, A., Hammarstrom, M., Johansson, I., Kotenyova, T., Nilsson, M., Nordlund, P., et al. (2008). The use of systematic N- and C-terminal deletions to promote production and structural studies of recombinant proteins. Protein Expr. Purif. *58*, 210–221.

Groves, M.R., Hanlon, N., Turowski, P., Hemmings, B.A., and Barford, D. (1999). The structure of the protein phosphatase 2A PR65/A subunit reveals the conformation of its 15 tandemly repeated HEAT motifs. Cell *96*, 99–110.

Grzesiek, S., Stahl, S.J., Wingfield, P.T., and Bax, A. (1996). The CD4 determinant for downregulation by HIV-1 Nef directly binds to Nef. Mapping of the Nef binding surface by NMR. Biochemistry *35*, 10256–10261.

Guo, F., Stanevich, V., Wlodarchak, N., Sengupta, R., Jiang, L., Satyshur, K.A., and Xing, Y. (2014). Structural basis of PP2A activation by PTPA, an ATP-dependent activation chaperone. Cell Res. *24*, 190–203.

Heijman, J., Dewenter, M., El-Armouche, A., and Dobrev, D. (2013). Function and regulation of serine/threonine phosphatases in the healthy and diseased heart. J. Mol. Cell Cardiol. *64*, 90–98.

Huhn, J., Jeffrey, P.D., Larsen, K., Rundberget, T., Rise, F., Cox, N.R., Arcus, V., Shi, Y., and Miles, C.O. (2009). A structural basis for the reduced toxicity of dinophysistoxin-2. Chem. Res. Toxicol. *22*, 1782–1786.

Hunter, T. (1995). Protein kinases and phosphatases: the yin and yang of protein phosphorylation and signaling. Cell *80*, 225–236.

Ikehara, T., Ikehara, S., Imamura, S., Shinjo, F., and Yasumoto, T. (2007). Methylation of the C-terminal leucine residue of the PP2A catalytic subunit is unnecessary for the catalytic activity and the binding of regulatory subunit (PR55/B). Biochem. Biophys. Res. Commun. *354*, 1052–1057.

Janssens, V. and Goris, J. (2001). Protein phosphatase 2A: a highly regulated family of serine/threonine phosphatases implicated in cell growth and signalling. Biochem. J. *353*, 417–439.

Janssens, V., Longin, S., and Goris, J. (2008). PP2A holoenzyme assembly: in cauda venenum (the sting is in the tail). Trends Biochem. Sci. *33*, 113–121.

Jiang, L., Stanevich, V., Satyshur, K.A., Kong, M., Watkins, G.R., Wadzinski, B.E., Sengupta, R., and Xing, Y. (2013). Structural basis of protein phosphatase 2A stable latency. Nat. Commun. *4*, 1699.

Johnson, B.A. and Blevins, R.A. (1994). NMR View: a computer program for the visualization and analysis of NMR data. J. Biomol. NMR *4*, 603–614.

Kabsch, W. (2010). XDS. Acta Crystallogr. D *66*, 125–132.

Lambrecht, C., Haesen, D., Sents, W., Ivanova, E., and Janssens, V. (2013). Structure, regulation, and pharmacological modulation of PP2A phosphatases. Methods Mol. Biol. *1053*, 283–305.

Leulliot, N., Vicentini, G., Jordens, J., Quevillon-Cheruel, S., Schiltz, M., Barford, D., van Tilbeurgh, H., and Goris, J. (2006). Crystal structure of the PP2A phosphatase activator: implications for its PP2A-specific PPIase activity. Mol. Cell *23*, 413–424.

Löw, C., Jegerschold, C., Kovermann, M., Moberg, P., and Nordlund, P. (2012). Optimisation of over-expression in *E. coli* and biophysical characterisation of human membrane protein synaptogyrin 1. PLoS One *7*, e38244.

Magnusdottir, A., Stenmark, P., Flodin, S., Nyman, T., Kotenyova, T., Graslund, S., Ogg, D., and Nordlund, P. (2009). The structure of the PP2A regulatory subunit B56γ: the remaining piece of the PP2A jigsaw puzzle. Proteins *74*, 212–221.

McCoy, A.J., Grosse-Kunstleve, R.W., Adams, P.D., Winn, M.D., Storoni, L.C., and Read, R.J. (2007). Phaser crystallographic software. J. Appl. Crystallogr. *40*, 658–674.

Mumby, M.C. and Walter, G. (1993). Protein serine/threonine phosphatases: structure, regulation, and functions in cell growth. Physiol. Rev. *73*, 673–699.

Ogris, E., Du, X., Nelson, K.C., Mak, E.K., Yu, X.X., Lane, W.S., and Pallas, D.C. (1999). A protein phosphatase methylesterase (PME-1) is one of several novel proteins stably associating with two inactive mutants of protein phosphatase 2A. J. Biol. Chem. *274*, 14382–14391.

Quistgaard, E.M., Nordlund, P., and Löw, C. (2012). High-resolution insights into binding of unfolded polypeptides by the PPIase chaperone SlpA. FASEB J. *26*, 4003–4013.

Rempola, B., Kaniak, A., Migdalski, A., Rytka, J., Slonimski, P.P., and di Rago, J.P. (2000). Functional analysis of RRD1 (YIL153w) and RRD2 (YPL152w), which encode two putative activators of the phosphotyrosyl phosphatase activity of PP2A in *Saccharomyces cerevisiae*. Mol. Gen. Genet. *262*, 1081–1092.

Sablina, A.A., Hector, M., Colpaert, N., and Hahn, W.C. (2010). Identification of PP2A complexes and pathways involved in cell transformation. Cancer Res. *70*, 10474–10484.

Schmitz, M.H., Held, M., Janssens, V., Hutchins, J.R., Hudecz, O., Ivanova, E., Goris, J., Trinkle-Mulcahy, L., Lamond, A.I., Poser, I., et al. (2010). Live-cell imaging RNAi screen identifies PP2A-B55alpha and importin-β1 as key mitotic exit regulators in human cells. Nat. Cell Biol. *12*, 886–893.

Sents, W., Ivanova, E., Lambrecht, C., Haesen, D., and Janssens, V. (2013). The biogenesis of active protein phosphatase 2A holoenzymes: a tightly regulated process creating phosphatase specificity. FEBS J. *280*, 644–661.

Shi, Y. (2009a). Assembly and structure of protein phosphatase 2A. Sci. China C Life Sci. *52*, 135–146.

Shi, Y. (2009b). Serine/threonine phosphatases: mechanism through structure. Cell *139*, 468–484.

Stanevich, V., Jiang, L., Satyshur, K.A., Li, Y., Jeffrey, P.D., Li, Z., Menden, P., Semmelhack, M.F., and Xing, Y. (2011). The structural basis for tight control of PP2A methylation and function by LCMT-1. Mol. Cell *41*, 331–342.

Tsai, M.L., Cronin, N., and Djordjevic, S. (2011). The structure of human leucine carboxyl methyltransferase 1 that regulates protein phosphatase PP2A. Acta Crystallogr. D *67*, 14–24.

Virshup, D.M. and Shenolikar, S. (2009). From promiscuity to precision: protein phosphatases get a makeover. Mol. Cell *33*, 537–545.

Weigelt, J. (1998). Single scan, sensitivity- and gradient-enhanced TROSY for multidimensional NMR experiments (vol 120, pg 10778, 1998). J. Am. Chem. Soc. *120*, 12706–12706.

Wlodarchak, N., Guo, F., Satyshur, K.A., Jiang, L., Jeffrey, P.D., Sun, T., Stanevich, V., Mumby, M.C., and Xing, Y. (2013). Structure of the Ca^{2+}-dependent PP2A heterotrimer and insights into Cdc6 dephosphorylation. Cell Res. *23*, 931–946.

Woestenenk, E.A., Hammarstrom, M., van den Berg, S., Hard, T., and Berglund, H. (2004). His tag effect on solubility of human proteins produced in *Escherichia coli*: a comparison between four expression vectors. J. Struct. Funct. Genomics *5*, 217–229.

Wurzenberger, C. and Gerlich, D.W. (2011). Phosphatases: providing safe passage through mitotic exit. Nat. Rev. Mol. Cell Biol. *12*, 469–482.

Xing, Y., Xu, Y., Chen, Y., Jeffrey, P.D., Chao, Y., Lin, Z., Li, Z., Strack, S., Stock, J.B., and Shi, Y. (2006). Structure of protein phosphatase 2A core enzyme bound to tumor-inducing toxins. Cell *127*, 341–353.

Xing, Y., Li, Z., Chen, Y., Stock, J.B., Jeffrey, P.D., and Shi, Y. (2008). Structural mechanism of demethylation and inactivation of protein phosphatase 2A. Cell *133*, 154–163.

Xu, Y., Xing, Y., Chen, Y., Chao, Y., Lin, Z., Fan, E., Yu, J.W., Strack, S., Jeffrey, P.D., and Shi, Y. (2006). Structure of the protein phosphatase 2A holoenzyme. Cell *127*, 1239–1251.

Xu, Y., Chen, Y., Zhang, P., Jeffrey, P.D., and Shi, Y. (2008). Structure of a protein phosphatase 2A holoenzyme: insights into B55-mediated Tau dephosphorylation. Mol. Cell *31*, 873–885.